remote sensing

MDPI

Article

A Cognitive Beamforming Method via Range-Doppler Map Features for Skywave Radar

Zhenshuo Lei [1,2], Hui Chen [2], Zhaojian Zhang [2], Gaoqi Dou [1] and Yongliang Wang [2,*]

[1] School of Electronic Engineering, Naval University of Engineering, Wuhan 430033, China; 14213066@bjtu.edu.cn (Z.L.); hjgcqq@163.com (G.D.)
[2] Department of Early Warning Technology, Wuhan Early Warning Academy, Wuhan 430019, China; chhglr@sina.com (H.C.); zzj554038@163.com (Z.Z.)
* Correspondence: ylwangkjld@163.com

Abstract: For skywave over-the-horizon radar, beamforming techniques are often used to suppress airspace radio frequency interference because the high-frequency band is shared by many devices. To address the problems that the traditional beamforming method is not capable of recognizing the electromagnetic environment and that its performance is greatly affected by the accuracy of signal feature estimation, a cognitive beamforming method using range-Doppler (RD) map features for skywave radar is proposed. First, the RD map is weighted by a local attention model, and then, texture features are extracted as the inputs to a support vector machine. Finally, the support vector machine is used to predict the optimal diagonal loading factor. Simulation results show that the output signal-to-interference-plus-noise ratio is improved compared with previous methods. The proposed method is suitable for many kinds of common unsatisfactory scenarios, making it beneficial for engineering implementation.

Keywords: cognitive beamforming; skywave over-the-horizon radar (OTHR); range-Doppler (RD) map; attention model; support vector machine

Citation: Lei, Z.; Chen, H.; Zhang, Z.; Dou, G.; Wang, Y. A Cognitive Beamforming Method via Range-Doppler Map Features for Skywave Radar. *Remote Sens.* **2022**, *14*, 2879. https://doi.org/10.3390/rs14122879

Academic Editors: Jingwei Xu, Keqing Duan, Weijian Liu and Xiongpeng He

Received: 11 May 2022
Accepted: 14 June 2022
Published: 16 June 2022

1. Introduction

Skywave over-the-horizon radar (OTHR) works in the high-frequency (HF) band (3–30 MHz) [1,2], where ionospheric reflection is most significant, and can overcome the influence of the curvature of the earth to enable the detection of targets beyond the horizon [3–5]. However, due to the large amount of civil equipment operating at similar frequencies and the complex electromagnetic environment in its working frequency band, OTHR is highly susceptible to all kinds of radio frequency interference (RFI) [6]. The existence of interference seriously affects the detection ability of radar; therefore, it is necessary to suppress interference as part of front-end signal processing. Beamforming, a conventional interference suppression method, can reduce the receiving gain of the signal in the direction of the interference by weighting the signal from the receiving array. This is widely considered useful because it can suppress RFI in nontarget directions in the airspace [7]. In skywave OTHR application scenarios, diagonal loading (DL) beamformers [8] are often used as a simple and effective means of improving the RFI suppression effect under non-ideal conditions. The DL technique can not only suppress the influence of small eigenvalues on the adaptive weight vector to accelerate the convergence of an adaptive beamformer, but also suppress the influence of direction-of-arrival (DOA) mismatches to avoid signal cancellation. Therefore, this technique is often used in robust beamforming algorithms. However, the difficulty in determining the DL factor (DLF) limits the practical capabilities of such a beamformer [9]. More seriously, DL beamformers without cognitive ability face great challenges from new interference technologies, flexible interference strategies and combinations of various interference methods.

In recent years, many methods for automatic DLF selection were proposed. Yu et al. [10] calculated the DL level automatically using the spatial matching method. Ideally, the DLF obtained via this method should make the noise eigenvalues approximately equal while ensuring that the interference eigenvalues are less affected. However, when the desired signal power is equal to or greater than the interference power, the interference eigenvalues would be more strongly affected, leading to a decrease in the zero depth of the beam pattern and thus a weakening of the interference suppression effect. The variable DL method was proposed in reference [11]. Under the constraints of suppressing small eigenvalue disturbances and effectively reducing the expected signal proportion in the covariance matrix, the minimum DLF is taken to improve beamforming robustness. However, in this method, the minimum DLF was set based on the noise power. Consequently, the results depended on estimating the statistical signal characteristics, which is a limitation. In reference [12], the loading values were calculated according to the characteristic structure of the covariance matrix. The idea was to use DL technology at a low signal-to-noise ratio (SNR) but not at a high SNR. The resulting beamforming effect was good under high- and low-SNR conditions, and was improved under small quick beat conditions. However, the method was greatly affected by the number of sensor elements, and its performance was poor when the dimensions of the target source and interference source were much smaller than the number of elements. Song et al. [13] proposed an automatic DL method based on the minimum mean square error (MMSE) criterion. By estimating the covariance matrix more accurately, the problem of performance degradation when the number of fast beats is large was solved. However, the effect of the number of elements on the DL quantity is not considered in this method, similar to the method in [12]. The method proposed by Xiao et al. [14] could be used to deduce the value range of the optimal diagonal load with a change in the input signal, thereby achieving an adaptive effect while increasing the optimization efficiency. However, this method determines only the optimal interval and does not accurately calculate the final value, so there is still a need to traverse the possible values or rely on human experience for selection.

Although promising studies on automatic calculation methods for DL have been reported in recent years, most of them depend on prior knowledge of the signal characteristics or require a specific application environment. This kind of anti-interference thinking that does not consider environmental perception ability does not agree with the development trend in electronic warfare. As the concept of cognitive electronic warfare advances, future radar should be able to actively recognize and accurately understand the interference of different degrees in an actual battlefield environment and then adjust the means or specific parameters of anti-interference. To address these shortcomings, Luo et al. [15] proposed that range-Doppler (RD) image features could be used to perceive the current electromagnetic environment. Roughness was used as an index to evaluate the RD maps in an OTHR system. A feedback system was established, and the optimal DLF was obtained through traversal search. The experimental results show that there was a close relationship between RD image features and the electromagnetic environment, which provides a new method for solving the OTHR interference suppression problem. However, the discriminative effect of roughness as a single index is limited, and there are no good value rules for the step size or the optimization range to be traversed, which are important factors affecting the performance of the method.

Inspired by reference [15], we considered using a machine learning method to build the mapping relationship between the RD map features and the optimal DLF, with the aim of enabling the radar system to acquire the cognitive ability to better suppress complex and changeable RFI. At the same time, Tamura texture features were introduced to analyze the gray distribution characteristics of the pixels and their surrounding spatial neighborhood in six dimensions, namely, coarseness, contrast, directionality, linearity, regularity and roughness, to further improve the ability to analyze visual clues. The goals of this study include the following.

(1) We propose a cognitive beamforming method via RD map features (RDF-CB) for skywave radar. Unlike traditional OTHR signal processing methods [10–14], the prior knowledge used in the proposed method is not limited to the current electromagnetic environment. Therefore, this method does not completely rely on accurately estimating the a priori information of the current signal characteristics or require the uncertainty of the current target orientation to satisfy certain assumptions; that is, it can adjust itself by sensing the current electromagnetic environment.

(2) This paper uses machine learning to predict the DLF through regression and solves the regression function in Hilbert space to avoid the influence of subjective factors on optimal DLF selection. In contrast, the purpose of Tamura texture feature extraction in reference [15] was to conduct DLF traversal optimization based on the strong correlation between the monotonicity of the roughness and the monotonicity of the output signal-to-interference-plus-noise ratio (SINR). Although this solves the problem of the difficulty in determining the DLF to a certain extent, the selection criteria for the search interval and the search step length were not further explained, meaning that DLF selection still ultimately relies on human experience. A larger search interval and a smaller search step length reduce the processing speed, while a smaller interval and a larger step length adversely affect the accuracy. Therefore, the method presented in this paper can better meet the requirements for cognitive electronic warfare.

(3) In the method proposed here, multidimensional texture features can be effectively used to describe RD maps more completely. In contrast, in the method from reference [15], other texture features were not applicable because of the weak correlation between their monotonicity and the monotonicity of the output SINR. This method of extracting only one-dimensional features tends to result in a loss in detail from the RD map, leading to reduced input information. Moreover, an attention model based on information entropy is introduced in this paper based on the characteristics of the OTHR RD map, thereby suppressing feature weights in areas with high similarity between classes while highlighting key information.

The rest of this article is organized as follows. In Section 2, considering the particularities of skywave OTHRs, an RD map feature extraction method is introduced. And then, we describes how to construct a cognitive DL beamformer using a trained support vector machine (SVM). Section 3 introduces the experimental results and analyses. Discussion are presented in Section 4, and conclusions are drawn in Section 5.

2. Materials and Methods

2.1. Skywave OTHR RD Map

When analyzing the signal processing results of skywave OTHRs, the elements in the RD matrix are usually modulated and visualized based on relative amplitude to form the RD map. The main components of the echo signal, such as the target, sea clutter, interference and noise, can be found in the corresponding regions in the RD map, as shown in Figure 1. In this paper, the RD map shows OTHR measurements before coordinate registration (CR) processing rather than the real location of the target.

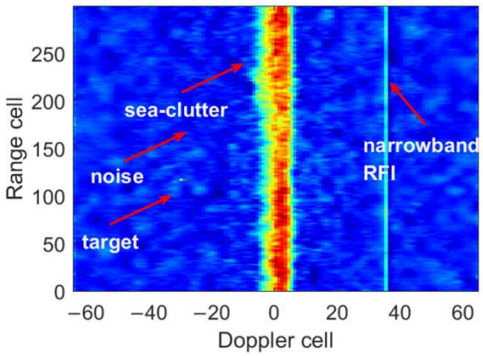

Figure 1. The target, sea clutter and narrowband RFI regions in an OTHR RD map.

An important prerequisite for obtaining a good beamforming effect is accurate perception of the current electromagnetic environment. The selection of key parameters and the application of specific technologies need to match the current electromagnetic environment. This can be done by analyzing RD maps' information. Taking the DL beamformer as an example, the selection of the DLF depends on the accuracy of the estimation of the sample covariance matrix. By observing the RD map after conventional signal processing, we can distinguish whether the current estimate of the covariance matrix is accurate, how accurate it is, and whether the cause is too few snapshots or a mismatch with the desired signal steering vector. For example, in Figure 2, Figure 2a shows the ideal case, in which the target is clearly visible and the interference noise is effectively suppressed. In contrast, in Figure 2b,c, the target echo is weak and the interference noise suppression is poor, with more residue. It can be said that the observation and analysis of the RD map is an important link in the OTHR signal processing chain, and can provide information feedback for optimizing the signal processing algorithm. Therefore, it is theoretically feasible for skywave OTHRs to acquire cognitive anti-interference capability by analyzing RD map features. However, there are two difficulties in the analysis of RD maps.

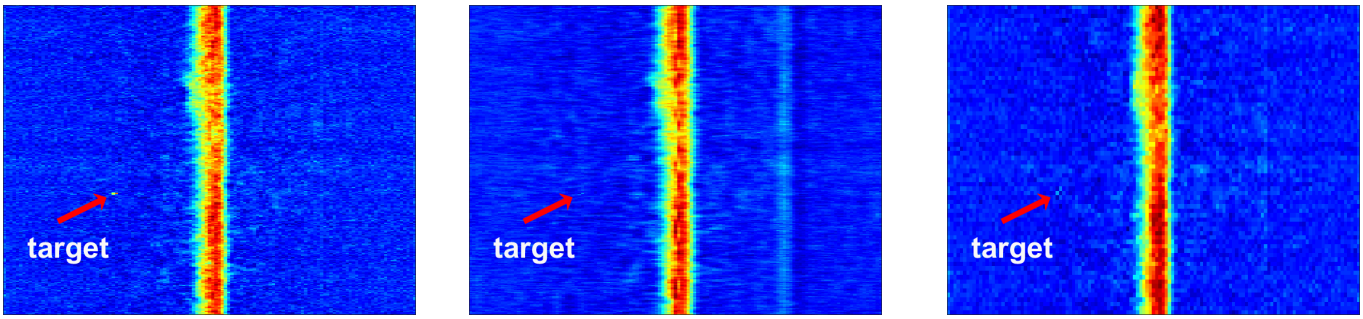

(**a**) (**b**) (**c**)

Figure 2. RD maps after conventional SMI processing: (**a**) 300 snapshots in the absence of mismatch; (**b**) 300 snapshots in the presence of mismatch, and (**c**) 70 snapshots in the absence of mismatch.

First, by observing a typical RD map for skywave OTHRs, we find that when the detection area and the target behavior are relatively fixed, an image of this kind can be divided into four regions: the sea-clutter region, located near the center of the Doppler coordinate axis; the interference region, where RFI often occurs; the target region, where target points often occur; and the noise base region, which covers the whole image, as shown in Figure 1. To better characterize the electromagnetic environment in which the current signal is located, it is necessary to distinguish the value of the information provided by different regions and focus on information from high-value regions. For example, in the RFI suppression process, the DLF is closely related to the noise base region and the RFI region, which exhibit sharp changes, whereas it is less related to the sea-clutter region, which exhibits relatively small changes, and the target region, which is often covered by interference or noise.

Second, although the RD map contains a large amount of data, due to its excessive number of pixels and large amount of miscellaneous information, direct use of the RD map itself will not only slow down subsequent processing but also obscure key information.

2.2. RD Map Feature Extraction for Skywave OTHR

To solve the two difficulties in applying RD maps to perception of the electromagnetic environment, this section proposes an RD map feature extraction method for skywave OTHRs. The feature extraction process is divided into two steps. In the first step, the RD map is converted into a grayscale image, and an information entropy attention model is introduced to weight the pixels of the grayscale RD image to give more attention to important areas in the RD map. The second step is to extract Tamura texture features of the weighted grayscale RD image and combine them into feature vectors. By simulating the

process of observing RD maps with the human eye to obtain intuitive reference information, the information contained in the RD maps can be quantified.

2.2.1. Attention Model Based on Information Entropy

To measure the importance of information in different regions of RD maps, a local attention model from the computer's vision field is proposed. This model can assign different weights to the pixels contained in each region according to their importance; that is, it can give more attention to features originating from regions with significant category differentiability. In this way, regional features with high similarity among classes can be suppressed to some extent to improve the cognitive ability to detect the electromagnetic environment.

Since the area of focus may change dramatically across the entire sample base, the information entropy, which represents the complexity and disorder of a system, is used to design the attention weight for each pixel [16]. The larger the information entropy value of the pixels is, the more drastic the variations in the pixels in the RD map sample base are. More attention should be given to key areas with drastic pixel changes, which is beneficial for increasing subsequent DLF prediction accuracy. The proposed local attention model based on information entropy is shown in Figure 3.

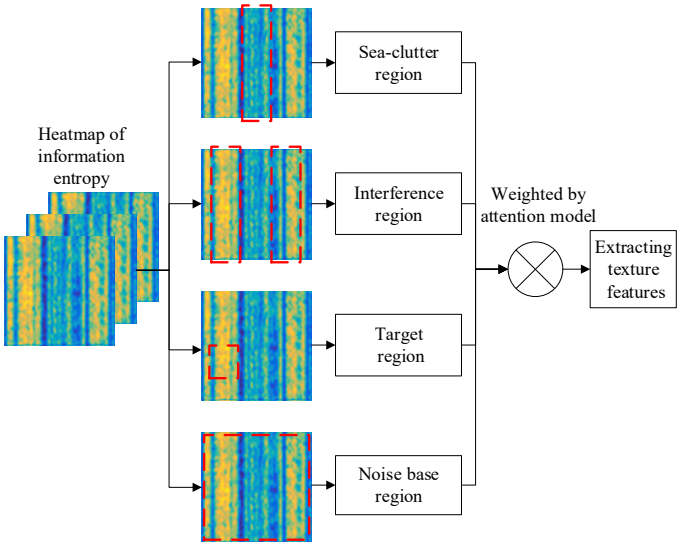

Figure 3. Local attention weighting model.

To enhance details in the low-power area of the RD map, it is necessary to avoid the high-intensity clutter occupying a high proportion of the grayscale range. Here, a logarithmic transformation method is used to transform the RD map into a grayscale graph, expand the low-amplitude part and compress the high-gray-value part. All elements in the RD map are denoted $Z_{m,n}$ after the modulo operation, and the RD gray image obtained after logarithmic transformation is expressed as

$$M_{v,n} = e \times \log_{d+1}(1 + d|Z_{v,n}|) \tag{1}$$

where d and e are constants used to control the degree of gray value transformation, $v = 1, L, V$ is the number of sensor elements, and $n = 1, \cdots, N$ is the number of snapshots.

Let a finite number of random variables $\{A(r)\}(r = 1, 2, \cdots, R)$ represent the random states of an uncertain system, where R is the number of RD map samples. Consider each pixel in the RD diagram to be an uncertain system. The information entropy of a pixel point (i, j) is expressed as

$$H_e(i, j) = -\sum_{r=1}^{R} P_{r(i,j)} \log_2 P_{r(i,j)} \tag{2}$$

where P_r is the probability of $A(r)$ occurring.

Information entropy is used to weight the gray values of the pixel points to focus attention on the key areas of the RD map, which is expressed as

$$f_H(i,j) = [1 + \eta H_e(i,j) w_e(i,j)] f(i,j) \tag{3}$$

where η is a constant used to control the degree of attention weighting, which takes a value of 0.1 in this paper. In the context of this paper, the reasonable value range of η nan be set to 0–0.5. When η is 0, the method degrades and the attentional mechanism does not affect the result. When η is higher than 0.5, the attention weighting model has a negative effect on real-time feature analysis ability. In other scenarios, the Pearson correlation coefficient can be introduced to analyze the specific situation. $w_e(i,j)$ is the attention weighting threshold, and $f(i,j)$ is the original gray value of pixel (i,j). If the information entropy of a pixel is larger than the upper quartile of the information entropy of all pixels in the RD map, the attention weighting threshold is set to 1; otherwise, it is set to 0. In other words, only the pixels with the highest information entropy are compensated, while pixels with lower information entropy are kept at their original values.

2.2.2. Tamura Texture Features

Tamura texture features [17] form the basis of a digital image texture expression method proposed by Tamura et al. They quantify the human visual perception of textures from the perspective of psychology and are widely used in pattern recognition and computer vision [18,19]. These texture features are divided into six types: coarseness, contrast, directionality, linearity, regularity and roughness. The texture features of the RD map can reflect the current electromagnetic environment, which is difficult to measure directly. Since the selection of key parameters and the application of specific technologies in beamforming are closely related to the perception of the electromagnetic environment, this inspired us to break away from the constraints of the traditional radar signal processing framework and seek a better suppression effect for OTHR RFI in the airspace from the perspective of image processing.

(1) Coarseness. Coarseness, which is the most basic texture feature, reflects the granularity of the image texture. Images with high coarseness exhibit obvious graininess. The specific calculation steps are as follows. First, the average intensity of the pixels near point (v', n') in the image is calculated with a movable window of $2^k \times 2^k$ pixels in size; this calculation is expressed as

$$A_k(v', n') = \sum_{i=v'-2^{k-1}}^{v'+2^{k-1}-1} \sum_{j=n'-2^{k-1}}^{n'+2^{k-1}-1} f_H(i,j)/2^{2k} \tag{4}$$

where k controls the size of the movable window and generally ranges from 2 to 6.

Then, the average intensity differences between nonoverlapping windows in the horizontal and vertical directions from each pixel point are calculated as follows:

$$E_{k,h}(v', n') = \left| A_k(v' + 2^{k-1}, n') - A_k(v' - 2^{k-1}, n') \right| \tag{5}$$

$$E_{k,g}(v', n') = \left| A_k(v', n' + 2^{k-1}) - A_k(v', n' - 2^{k-1}) \right| \tag{6}$$

where $E_{k,h}(v', n')$ is the difference in the horizontal direction and $E_{k,g}(v', n')$ is the difference in the vertical direction. For each pixel, let k_{best} be the value that maximizes the larger of $E_{k,h}(v', n')$ and $E_{k,g}(v', n')$; then, the corresponding optimal size can be expressed as

$$S_{best}(v', n') = 2^{k_{best}} \tag{7}$$

Finally, the coarseness is calculated as the average value of the optimal size for the whole image, which can be expressed as

$$F_{crs} = \frac{1}{V' \times N'} \sum_{v'=1}^{V'} \sum_{n'=1}^{N'} S_{best}(v', n') \tag{8}$$

where V' is the image width and N' is the image height.

(2) Contrast. Contrast reflects the local variation in the gray values of the image. The more obvious the difference among the gray values, the greater the contrast. The main influencing factors are the dynamic range of the gray values, the degree of polarization between black and white in the histogram, the sharpness of the edges and the cycle of repeating patterns. The contrast is calculated as

$$F_{con} = \frac{\sigma_{gray}^2}{u_4^{1/4}} \tag{9}$$

where μ_4 is the fourth moment of the gray values and σ_{gray} is the standard deviation of the gray values.

(3) Directionality. Directionality describes how textures are distributed or concentrated in certain directions. The calculation steps are as follows. First, the gradient vector at each pixel is calculated. The modulus and direction of this vector are expressed as

$$|\Delta E| = (|\Delta_H| + |\Delta_G|)/2 \tag{10}$$

$$\theta = \tan^{-1}(\Delta_G/\Delta_H) + \pi/2 \tag{11}$$

where Δ_H and Δ_G are the changes in the horizontal and vertical directions obtained by convolving the image with the following two 3×3 operators, respectively.

$$\begin{bmatrix} -1 & 0 & 1 \\ -1 & 0 & 1 \\ -1 & 0 & 1 \end{bmatrix} \begin{bmatrix} 1 & 1 & 1 \\ 0 & 0 & 0 \\ -1 & -1 & -1 \end{bmatrix}$$

After the gradient vectors of all pixel points have been calculated, the value of θ can be expressed based on the histogram H_D. This histogram is constructed by first discretizing the range of θ and then counting the number of pixels of each magnitude $|\Delta E|$ greater than a given threshold. The histogram forms peaks for strongly oriented images and is flat for nonoriented images. Finally, the overall directionality of the image can be obtained by calculating the sharpness of the peak values in the histogram; it is expressed as

$$F_{dir} = \sum_{p}^{n_p} \sum_{\Phi \in W_p} (\Phi - \Phi_p)^2 H_D(\Phi) \tag{12}$$

where p is the index of a peak in the histogram and n_p is the number of peaks in the histogram. For peak p, W_p represents all quantization regions contained in the peak, and Φ_p is the quantization region with the highest value.

(4) Linearity. Linearity refers to whether the image texture has a linear structure and is expressed as

$$F_{lin} = \frac{\sum_{i}^{r} \sum_{j}^{r} P_{Dd}(i,j) \cos[(i-j)\frac{2\pi}{r'}]}{\sum_{i}^{r} \sum_{j}^{r} P_{Dd}(i,j)} \tag{13}$$

where P_{Dd} is the $n' \times n'$ local direction co-occurrence matrix of points within a certain distance and r' is the number of dividing angles defining distinct directions, which is eight in this paper, specifically, up, down, left, right, left up, right up, left down and right down.

(5) Regularity. If the local texture of an image differs greatly from the overall texture, the image regularity is considered poor. The whole image is divided into several parts, and the variance in each subimage is calculated to obtain the regularity, which is expressed as

$$F_{reg} = 1 - \eta(\sigma_{crs} + \sigma_{con} + \sigma_{dir} + \sigma_{lin}) \tag{14}$$

where σ_{crs}, σ_{con}, σ_{dir} and σ_{lin} are the standard deviations of F_{crs}, F_{con}, F_{dir} and F_{lin}, respectively, and η_{reg} is a normalization factor. The value of η_{reg} in this paper is 0.0025. In different application scenarios, η_{reg} can be set according to the magnitude of standard deviation of different features. The ultimate goal is to get the standard deviation to the same order of magnitude as 1.

(6) Roughness. Roughness is the combination of coarseness and contrast. The roughness is expressed as

$$F_{rgh} = F_{crs} + F_{con} \tag{15}$$

The improvement effect of conventional beamforming on the quality of the RD map determines the value range of the corresponding DLF to a certain extent. Therefore, when constructing RD image feature vectors, not only are the six-dimensional Tamura texture features of the RD map after conventional beamforming calculated but also the difference values of the six-dimensional Tamura texture features of the RD maps before and after conventional beamforming. That is, the original RD map is transformed into a 12-dimensional feature vector.

2.3. Application of RD Map Features in DL Beamforming

RD map features can be used to perceive the current electromagnetic environment of the OTHR. This section presents an application example in which RD map features are used to construct a cognitive beamformer. DL is an effective and widely used adaptive beamforming technique. When RD map features and machine learning methods are applied to a DL beamformer, it becomes cognitively capable. That is, through the understanding of the current electromagnetic environment, the most appropriate DLF is determined to improve the ability of OTHR to perform airspace suppression of RFI and then improve the output SINR.

2.3.1. DL Beamformer

Most of the RFI encountered by skywave radars exhibits spatial directivity; therefore, we first considered suppressing such interference in the spatial domain. Specifically, a set of weight vectors was designed to beamform the received data of the array to ensure that the echo signal in the direction of the target could be received without loss while simultaneously suppressing the echo signal in the direction of interference.

Let the receiving array be a phased array with V sensor elements at half-wavelength spacing. The expression for the received data is

$$X(n) = [x_1(n), x_2(n), \cdots, x_V(n)]^T \tag{16}$$

where $n = 1, 2, \ldots, N$ is the number of snapshots and $x(n)$ is the received signal of the nth snapshot. When the skywave OTHR detects maritime targets, the received signal $x(n)$ is expressed as

$$x(n) = s(n) + c(n) + i'(n) + \sigma(n) \tag{17}$$

where $s(n)$ is the potential target echo, $c(n)$ is ocean clutter, $i'(n)$ is interference, and $\sigma(n)$ is noise.

Let the weight vector for beamforming be $w \in C^{V\times 1}$. For the received signal X, the output after beamforming is $y = w^H X$. The output corresponding to the nth snapshot is expressed as

$$y(n) = w^H x(n) \tag{18}$$

where $(\cdot)^H$ is the conjugate transposition of the matrix. If the true signal steering vector a is known, then the optimal weight vector obtained based on the minimum variance distortionless response (MVDR) criterion can be expressed as

$$w_{opt} = \mu \cdot R_{i+\sigma}^{-1} a \tag{19}$$

where $\mu = (a^H R_{i'+\sigma}^{-1} a)^{-1}$ is a normalization coefficient and $R_{i'+\sigma} = E[(i'_n + \sigma_n)(i'_n + \sigma_n)^H]$ is the interference-plus-noise covariance matrix. In practical applications, however, the accurate signal steering vector a and covariance matrix $R_{i'+\sigma}$ are typically unavailable, and the observed signal steering vector $\widetilde{a}$ and sample covariance matrix $\widetilde{R}$ are adopted as approximations. With these substitutions, the optimal weight vector is replaced with w_{SMI}:

$$w_{SMI} = (\widetilde{a}^H R^{-1} \widetilde{a})^{-1} \widetilde{R}^{-1} \widetilde{a} \tag{20}$$

where the resulting beamformer is known as a sample matrix inverse (SMI) beamformer. When the estimate of $\widetilde{R}$ is not accurate, the interference rejection performance of w_{SMI} will sharply decrease. In addition, when there is a matching deviation between $\widetilde{a}$ and a, w_{SMI} shows poor robustness.

To improve the interference suppression performance and robustness of SMI methods, DL beamformers are often used. The corresponding weight vector is expressed as

$$w_{DL} = (\widetilde{a}^H \widetilde{R}^{-1} \widetilde{a})^{-1} (\widetilde{R} + \beta I)^{-1} \widetilde{a} \tag{21}$$

where I is the identity matrix and β is the DLF. Under the premise of proper DLF selection, w_{DL} can yield better interference suppression performance than w_{SMI} and shows better robustness.

Initially, the selection of the DLF depended on human subjective experience. On this basis, researchers proposed several improved automatic selection methods [10–14]. However, these methods need to rely on a priori information concerning the statistical signal properties, or require the uncertainty of the steering vector to satisfy certain assumptions. Unfortunately, these assumptions are difficult to satisfy in OTHR systems. Therefore, for skywave OTHR applications, this paper proposes a new DLF calculation approach based on RD map features to improve the actual interference suppression performance of the weight vector w_{DL}.

2.3.2. SVM Prediction

After the RD map features have been extracted, a cognitive beamformer based on OTHR image features can be realized by incorporating a DLF prediction method. Machine learning is an effective method for numerical regression prediction. SVMs are commonly used machine learning models with a good learning effect on small samples and excellent generalization capabilities. Thus, for DLF regression prediction, the extracted RD map texture features weighted by local attention are used as the input to an SVM. The SVM is trained using known RD maps and the corresponding optimal DLFs to construct a knowledge base. In this way, the mapping relationship between the texture features of the RD map and the optimal DLF can be obtained, and the prediction of the optimal DLF corresponding to an unknown RD map can be realized.

The working principle of an SVM is to map sample data to a Hilbert space through a kernel function. It thus transforms a low-dimensional nonseparable problem into a high-dimensional problem in which the samples are linearly separable through the construction of a hyperplane. When determining the hyperplane, it should be ensured that the distance

between each sample and the hyperplane is as large as possible and that the classification error is as small as possible. For a regression prediction problem, an SVM can also construct a regression model in the Hilbert space and transform the problem of determining the optimal classification hyperplane into a dual problem, which is expressed as

$$\begin{aligned} \max w(a) = & -\frac{1}{2}\sum_{k,l}^{q}(a_k^* - a_k)(a_l^* - a_l)K(F_k, F_l) \\ & + \sum_{k=1}^{q}\beta_k(a_k^* - a_k) - \varepsilon\sum_{k=1}^{q}\beta_k(a_k^* + a_k) \\ & s.t. \sum_{k=1}^{q}(a_k^* - a_k) = 0 \end{aligned} \tag{22}$$

where F denotes the input variables, which, in this paper, are the texture features weighted by local attention, and β denotes the output variables, which, in this paper, are the optimal DLFs. w_{svm} is an adjustable weight vector, and ε is a relaxation variable. $0 \le a_k, a_k^*, a_l, a_l^* \le c$ are the Lagrange multipliers, with c being a penalty coefficient. K_{SVM} is the kernel function; in this paper, a linear kernel function is selected. $k, l = 1, 2, \cdots, q(k \ne l)$. The optimal Lagrange multipliers are obtained through a quadratic programming optimization algorithm, and the final regression function is expressed as

$$f_{SVM}(F) = \sum_{k=1}^{q}(a_k - a_k^*)K_{SVM}(F_k, F) + b \tag{23}$$

where b is the intercept threshold.

In summary, the processing scheme of the RDF-CB for skywave radar is shown in Figure 4 and the optimal DLFs prediction process is shown in Algorithm 1.

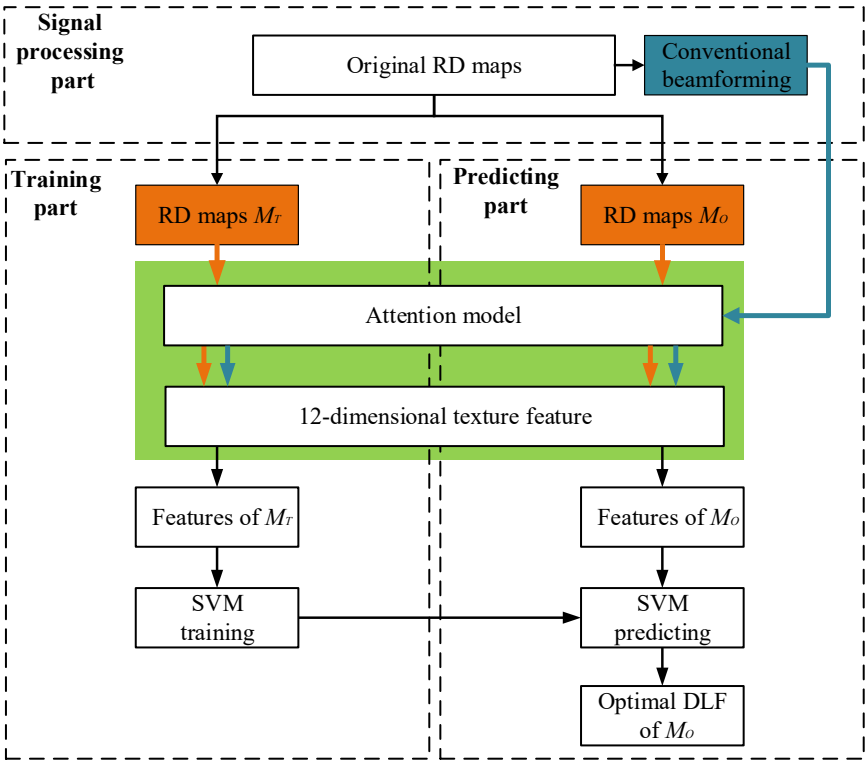

Figure 4. Signal processing scheme of the optimal DL beamformer based on RD map features.

Algorithm 1. Optimal DFLs prediction

Input: RD maps M_O for which the optimal DLFs are unknown, RD maps M_T for which the optimal DLFs are known, and labels (optimal DLFs) β_T corresponding to G_T.

Output: labels (optimal DLFs) β_O corresponding to M_O.

Step 1: Weight M_O and M_T (before and after conventional beamforming) with the local attention model.

Step 2: Calculate the 12-dimensional Tamura texture features of the weighted M_O and M_T to generate feature vectors F_O and F_T.

Step 3: Obtain the optimal DLFs β_T corresponding to F_T through the traversal method and use them as the training set labels for SVM training.

Step 4: Input F_O into the trained SVM.

Step 5: Obtain labels (optimal DLFs) β_O corresponding to F_O.

It should be noted that the knowledge base for the method presented in this paper is constructed based on accumulated historical data, and the optimal DLFs in the knowledge base can be obtained via the traversal method. Since model training is completed in the early preparation stage, it is not included in the specific steps of model application. Therefore, the selection of the search interval and search step length do not affect the real-time performance of the method.

3. Results

In this section, a measured radar echo signal mixed with a simulated interference signal was used as experimental data to verify the actual interference suppression effect of the proposed method. The target signal was a linear frequency modulation (LFM) signal coming from 0°. The interference components were narrowband RFI and broadband RFI coming from 10° and -5°, respectively. The noise was white noise. Each coherent integration time window contained 128 pulses. The penalty coefficient c and relaxation variable ε of SVM were optimized via particle swarm optimization. The sample library contained 100 samples with narrowband RFI, 100 samples with broadband RFI, 100 samples with both narrowband and broadband RFI, and 100 samples without RFI. Among them, 70% were randomly selected as the SVM training set, and the other 30% were selected as the SVM test set. To better demonstrate the effect of the proposed method, samples with both narrowband and broadband RFI are analyzed below. For all simulation examples, 200 Monte Carlo runs were performed to obtain the average results.

The RDF-CB proposed in this paper was compared with the beamforming method based on conjugate gradient algorithms (CG) [10], the beamforming method combined with the covariance matrix taper (CMT) [11], the beamforming method based on the characteristic structure of the covariance matrix (CS) [12], the general linear combination method (GLC) [13], and the beamforming method solved by the Lagrange multiplier (LM) [14]. Four examples are used to verify the performance of the RDF-CB approach.

Each of these methods has its own advantages. By estimating the steering vector and covariance matrix, CR causes the DLF to satisfy the following two conditions to the greatest possible extent in the ideal case: (1) the loaded noise eigenvalues should be approximately equal, and (2) the loaded interference eigenvalues should be minimally affected. The CMT method sets a lower bound on the DLF in accordance with the power of the noise. The establishment of this range, which relies on experience, helps the method achieve performance balanced between suppressing the interference of small eigenvalues and effectively reducing the expected signal in the covariance matrix. The CS method adopts the concept of a low SNR with no load and a high SNR with load. This method considers that DL should be carried out only when the interference value is much greater than the noise; in this way, the suppression of interference would not be affected. The principle of GLC is to obtain a more accurate estimated covariance matrix than the sample covariance matrix according to the MMSE criterion. In the LM method, an MVDR optimization model based on DL compensation is established, and the interval of the DLF is deduced on the basis of matrix theory. The aim is to achieve an adaptive effect while improving the optimization efficiency.

3.1. Comparison of Beam Patterns and RD Maps

In this section, the influence of DLF obtained by different methods on the signal processing results of skywave OTHRs was visually demonstrated using beam patterns and RD maps. The number of sensor elements was set to 32, the input SNR to 5 dB, the input interference to noise ratio to 20 dB and the DOA mismatch to 2°.

When the number of snapshots is 200, the beam patterns of the six approaches are shown in Figure 5. Figure 5a shows the beam patterns obtained after DL using the method in this paper. It can be seen that it had good performance improvement in both the beam sidelobe and interference nulls. The price is that the interference nulls became slightly shallower. However, since the nulls of the direction graph were deep enough, this would not have a great influence on interference suppression, which is also demonstrated by subsequent analysis combined with the output SINR. Figure 5b is the direction diagram obtained by CG. It had a low side lobe and nulls at the interference positions. However, when the nulls become shallow, the suppression ability of the strong interference signal would be greatly weakened, and the output SINR would be reduced. Similarly, Figure 5c shows that CMT possessed a weak ability to suppress interference. Its performance degradation was more serious and even produced deeper nulls in other directions. This is because DLF was too large, resulting in noise level "interference", so that the beam patterns in some directions formed "false alarm interference". Figure 5d shows the beam patterns corresponding to LM. Although the sidelobe was improved, it was still approximately 5 dB higher than Figure 5a. This is because the DLF was too small to effectively suppress the characteristic value disturbance of the noise. The performance of GLC, in Figure 5e, is similar to that of Figure 5a, and a better effect was obtained. However, performance degradation occurs when this method is applied to large arrays, which will be analyzed in the following sections. Figure 5f shows that, for LM, although the beam patterns obtained with a small DLF formed nulls aligned in the directions of interference, its sidelobe performance was poor. If main beam interference exists, the sidelobe level would be higher, and even the main beam would be distorted.

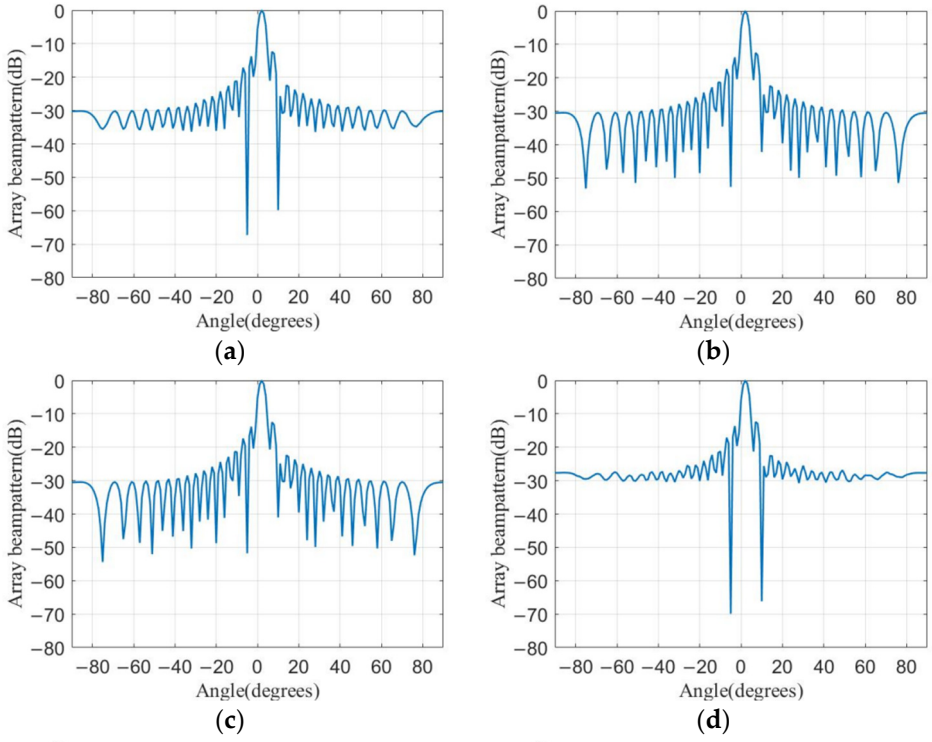

Figure 5. *Cont.*

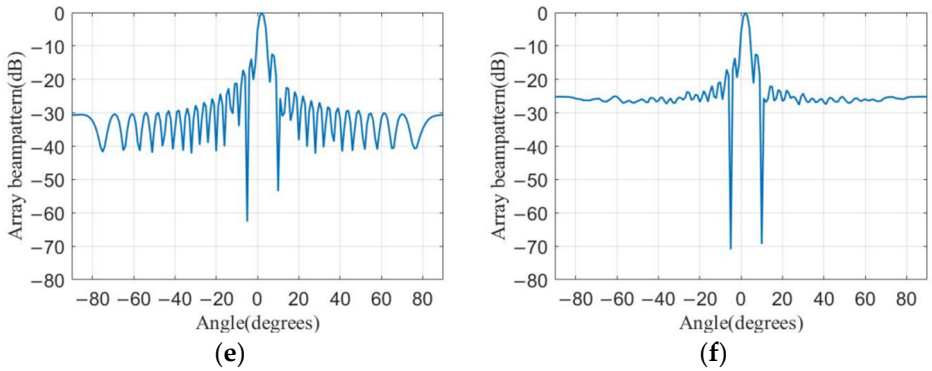

Figure 5. Beam patterns processed by six methods: (**a**) RDF-CB; (**b**) CG; (**c**) CMT; (**d**) CS; (**e**) GLC; (**f**) LM.

RD maps obtained by the six methods are shown in Figure 6. It can be seen that the method in this paper and GLC had good performance. After processing by other methods, the residual interference and strong noise in the RD maps affected target recognition. In Figure 6c, there were narrowband and wideband interferences that were not completely suppressed. In Figure 6b, there was weak narrowband interference near the −42nd Doppler channel. Compared with Figure 6a, this Doppler interference energy in Figure 6b was 3 dB higher on average. In Figure 6d,f, there were bright spots at the base that were easily mistaken for targets. For example, there was a bright spot located in the −61st Doppler channel, 83nd range channel. There was only a 5 dB energy gap between this bright spot and the target in Figure 6d, which was reduced to 3 dB in Figure 6f, but increased to 15 dB in Figure 6a.

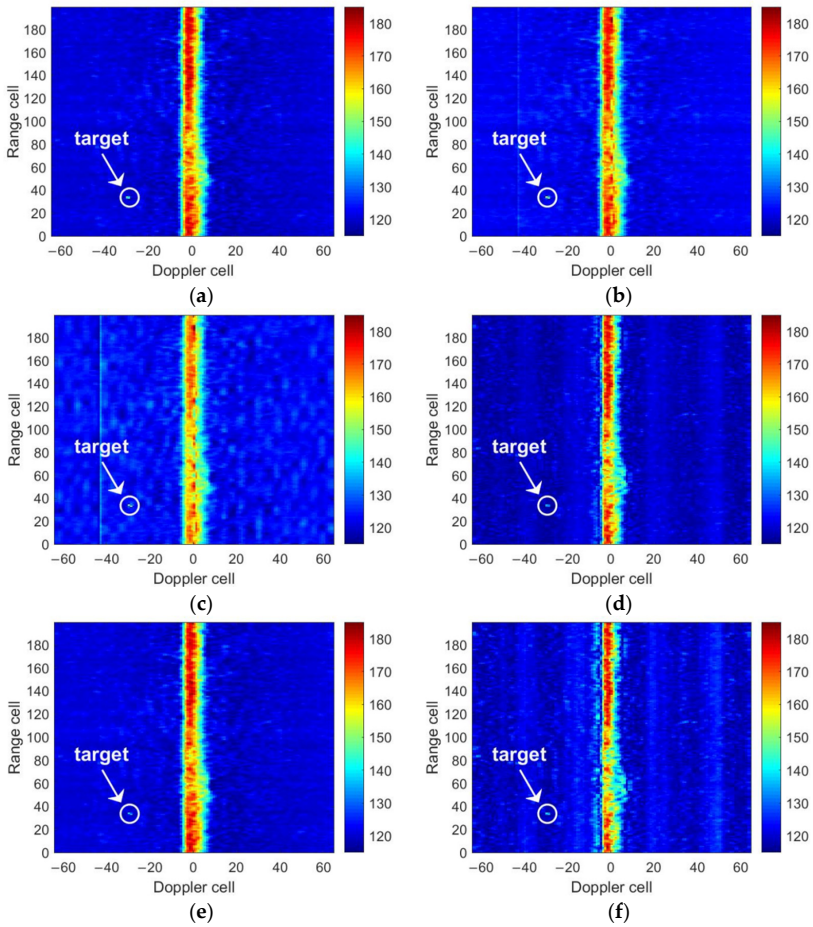

Figure 6. RD maps processed by six methods: (**a**) RDF-CB; (**b**) CG; (**c**) CMT; (**d**) CS; (**e**) GLC; (**f**) LM.

3.2. Impact of the Number of Snapshots and DOA Mismatches

A small number of snapshots and DOA mismatches are common nonideal conditions that influence the beamforming effect. The number of sensor elements was set to 32, the input SNR to 5 dB and the input interference to noise ratio to 20 dB.

On the premise that the DOA mismatch is 0°, we studied the changes in the DLF of each method as the number of snapshots increased, as shown in Figure 7. Theoretically, as the number of snapshots increases, the estimation of the covariance matrix should be more accurate, so the required DLF should be increasingly smaller until reaching a fixed value. All six methods showed correct variation trends, and their performance difference was mainly affected by whether the DLF was appropriate. When the DOA was mismatched, the DLF value could be reasonably adjusted by RDF-CB. The other five comparison methods all had poor perception ability in the mismatched situation and the corresponding DLF had almost no change.

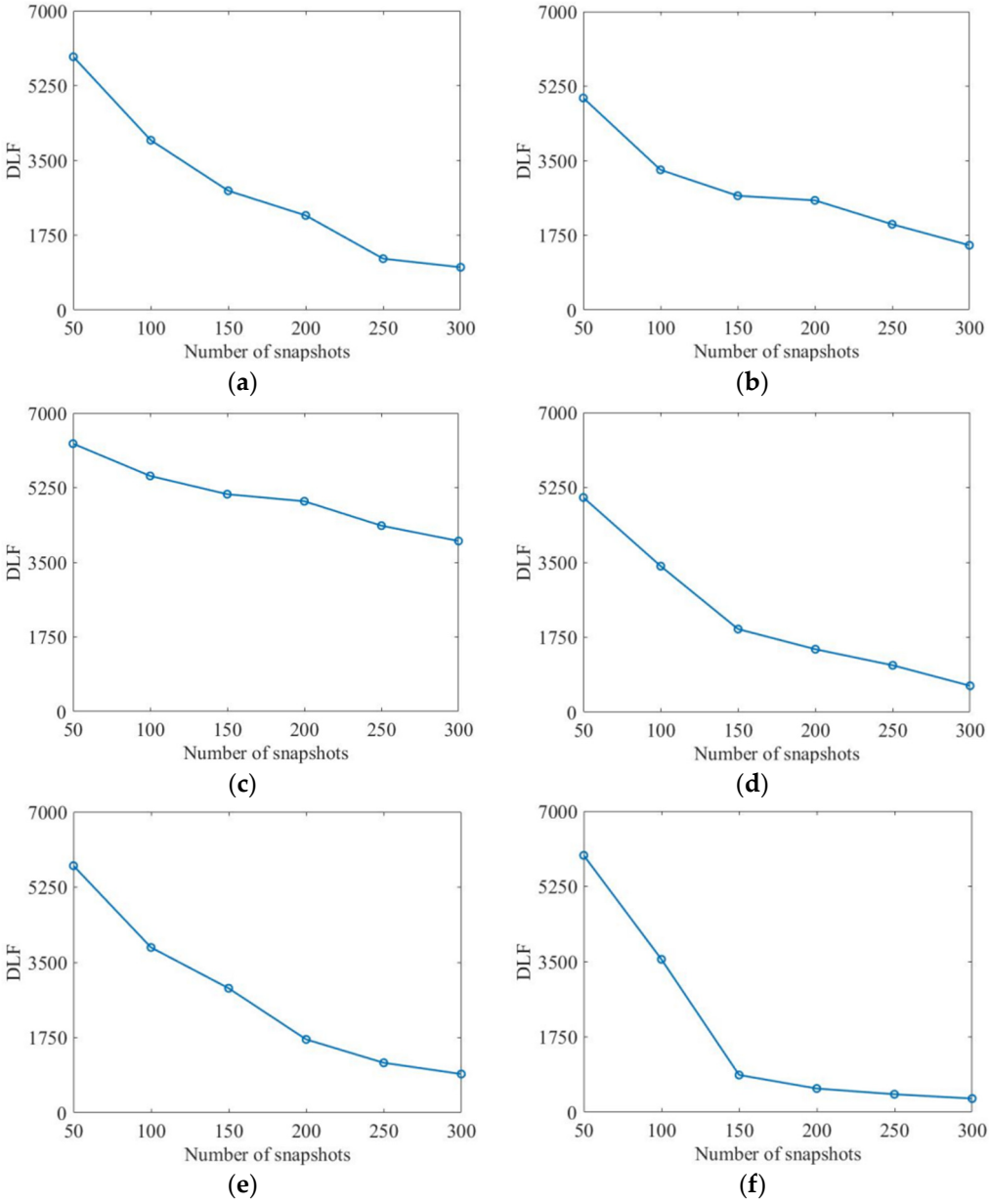

Figure 7. Comparison of average DLF versus the number of snapshots: (**a**) RDF-CB; (**b**) CG; (**c**) CMT; (**d**) CS; (**e**) GLC; (**f**) LM.

Figure 8 shows the variation trend in the output SINR with a number of snapshots ranging from 50 to 300 under two conditions: when the DOA is accurate and when the DOA mismatch is 2°.

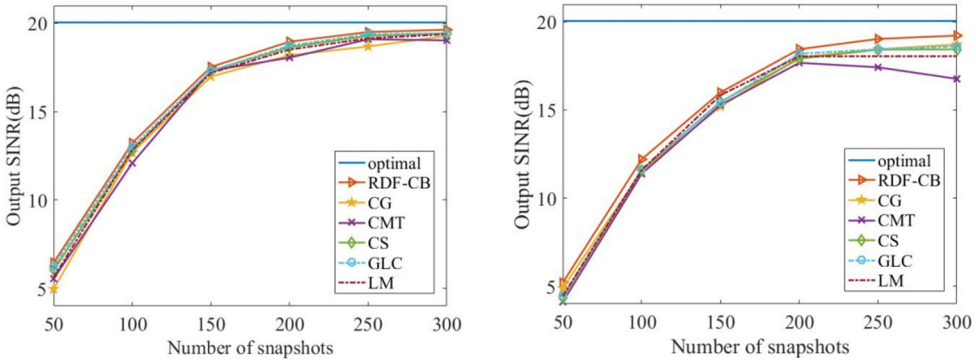

Figure 8. Output SINR versus number of snapshots: (**a**) in the absence of DOA mismatch; (**b**) in the presence of DOA mismatch.

Figure 8a,b are analyzed separately to summarize the influence of the number of snapshots on the output SINR of each compared method. RDF-CB had the best performance among the six methods. In the absence of DOA mismatch, CS and GLC showed performance close to that of RDF-CB. When the DOA mismatch was 2°, the performances of GLC and LM were close to those in this paper. In contrast, the performance of CG was poor because of the slow DLF adjustment speed. When the number of snapshots was large, the DLF of this method was too large, which affected the interference eigenvalues and led to a decrease in the null depth of the beam pattern. When the number of snapshots was close to the number of sensor elements, the DLF was not large enough to effectively suppress small eigenvalue disturbances. The DLF of CMT is dynamically adjusted based on the ratio between the square of the signal power and the square of the noise power, which made the DLF larger than in other methods in the case of few snapshots. An excessively large DLF would lead to overloading of the covariance matrix and reduce the output SINR. For LM, the optimal value range of the DLF is first calculated, and the final value of the DLF is then obtained through traversal. The performance was greatly affected by the search interval and the search step length, and the process of repeatedly traversing the values within the value range reduced the timeliness of this method.

By comparing Figure 8a,b, the influence of DOA mismatch on the output SINR of each method can be summarized. In the case of few snapshots, all methods were insensitive to DOA mismatch, and the output SINR changed little. When the number of snapshots was large, the performance of RDF-CB still did not change significantly with DOA mismatch; its output SINR decreased the least, by an average of 0.9 dB. This shows that RDF-CB exhibits good robustness and adaptability to DOA mismatch. In contrast, the other methods were limited by their traditional signal processing architecture, resulting in a significant drop in the output SINR.

The reason for the difference in performance is that the method in this paper can distinguish among different cases, including the number of snapshots and whether the DOA is mismatched, based on RD map features. Specifically, as the number of snapshots decreases, the resolution of the RD map decreases, the contrast significantly increases, and the directionality significantly decreases. In the presence of DOA mismatch, the difference values of the six-dimensional Tamura texture features of the RD maps before and after conventional beamforming are greatly different. Therefore, compared with the other methods, RDF-CB can achieve stable anti-interference performance under different conditions. Additionally, DLF prediction is performed in a data-driven manner based on a knowledge base for pretraining. Thus, it is possible to avoid the phenomenon of pursuing a high output SINR in one scenario at the expense of the method's performance in other scenarios.

3.3. Impact of the Input SNR

In practical beamforming applications, a low-input SNR is usually regarded as an undesirable condition. Here, the number of sensor elements was set to 32, and the number of snapshots was set to 150. Under the two conditions in which the DOA is accurate and the DOA mismatch is 2°, the variation trends in the output SINR with input SNR ranging from −10 dB to 10 dB are shown in Figure 9. Since DLF is used to suppress noise eigenvalue disturbance, when the input noise was fixed, the input power of the expected signal and the interfering signal had no obvious effect on DLF.

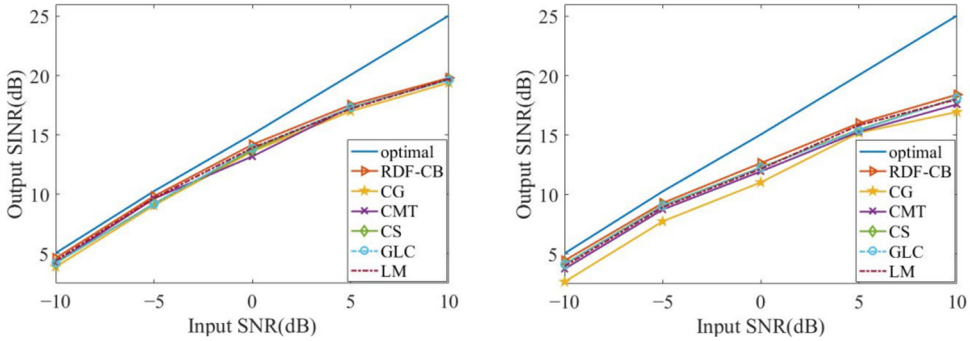

Figure 9. Output SINR versus input SNR: (**a**) in the absence of DOA mismatch and (**b**) in the presence of DOA mismatch.

It can be seen from this figure that the antijamming effects of each method were different; in particular, the method in this paper achieved better effects than the others. The reasons are as follows. CMT considers high- and low-input SNRs two distinct cases and defines two different DLF calculation methods accordingly. As a result, the performance of this method obviously degraded near the boundary between high- and low-input SNRs. CG still showed poor performance due to its slow DLF adjustment speed. Similarly, CS, which takes the average value of the eigenvalues as the basis for selecting the DLF, and GLC, which is limited by the MMSE criterion, also showed slight performance degradation due to their insufficient DLF adjustment range.

In this paper, an attention model based on information entropy was constructed to focus attention on texture features extracted from the noise base and RFI areas of the RD map, thus endowing the model with some cognitive ability regarding the current electromagnetic environment. After preliminary training, the model could select a suitable DLF that matches the current input SNR to improve the output SINR.

3.4. Impact of the Number of Sensor Elements

To analyze the robustness of each method in the case of a large array, the input SNR was set to 5 dB, the input interference to noise ratio to 20 dB, and the number of snapshots to 150. The relationship between the DLF and the number of elements is shown in Figure 10. The purpose of setting the number of elements in the range from 16 to 80 is to explore the possibility of using subarrays for detection in multiple areas simultaneously [20]. As the number of elements increased, the DLFs of CMT and CS decreased, while the DLFs of the other methods had the same change trend as the number of elements.

Under the two conditions in which the DOA is accurate and the DOA mismatch is 2°, the variation trends in the output SINR with the number of sensor elements ranging from 16 to 80 are shown in Figure 11.

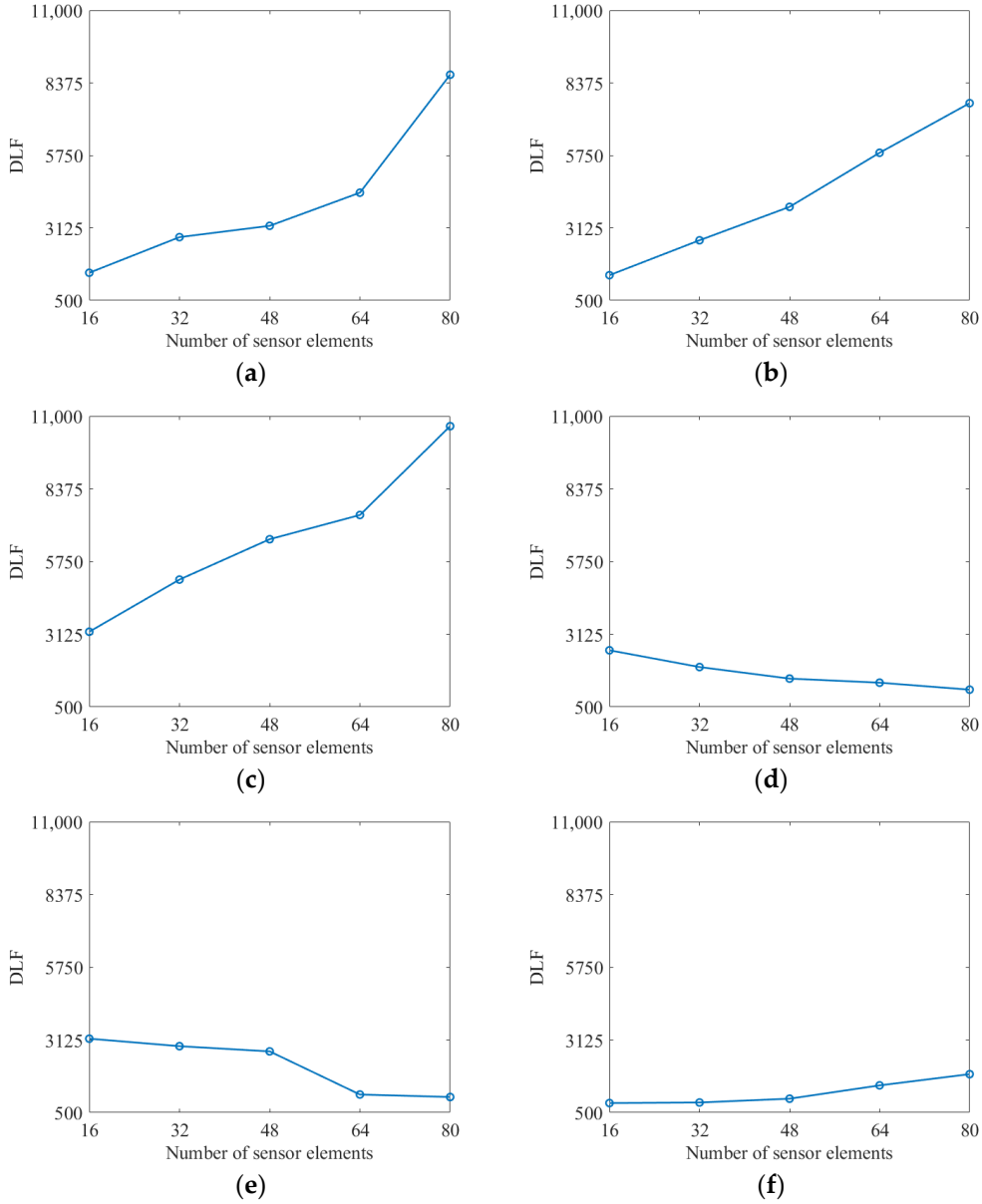

Figure 10. Comparison of average DLF versus the number of snapshots: (**a**) RDF-CB; (**b**) CG; (**c**) CMT; (**d**) CS; (**e**) GLC; (**f**) LM.

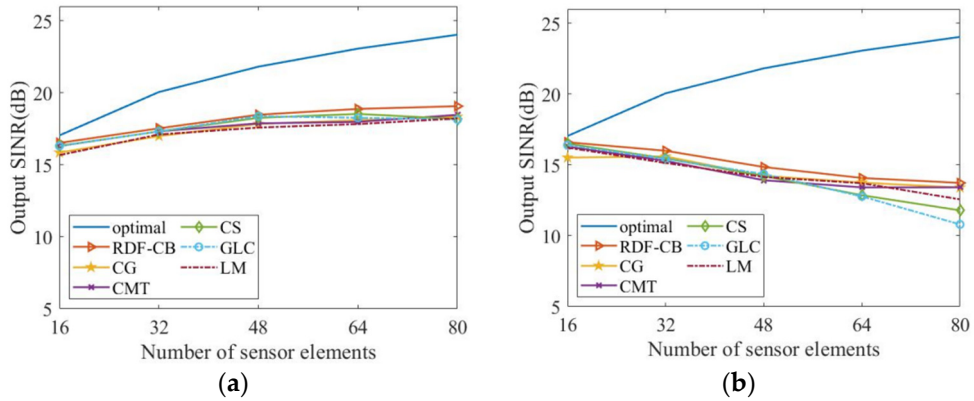

Figure 11. Output SINR versus the number of sensor elements: (**a**) in the absence of DOA mismatch and (**b**) in the presence of DOA mismatch.

In the absence of DOA mismatch, the performance of each method was similar. Among them, LM and CG still had a performance gap relative to RDF-CB due to the slow DLF adjustment speed. In the presence of DOA mismatch, the performance of each method was obviously different, especially in the case of a large number of sensor elements. Theoretically, the deviation between the sample covariance matrix and the true covariance matrix increases as the number of sensor elements increases. Therefore, the DLF should show an increasing trend to effectively compensate for the deviation in the covariance matrix. GLC does not consider the influence of the number of sensor elements on the DLF. In this method, restricted by the MMSE criterion, the DLF decreased as the number of sensor elements increased, resulting in degradation of the method's performance. CS uses the average value of the eigenvalues, which is greatly influenced by the number of elements, as a reference for DLF calculation. When the dimensions of the target source and interference source were much smaller than the number of sensor elements, the noise eigenvalue could not be corrected effectively, and the performance of the method was poor. In contrast, RDF-CB still showed high robustness as the number of sensor elements varied. The reason is that the increase in the sample covariance matrix deviation is reflected in the RD map, which leads to a change in texture features such as coarseness. Therefore, RDF-CB couldreasonably adjust the DLF according to this phenomenon.

In conclusion, under various common RFI environments, the RD map texture features weighted using an attention model can be used to predict the optimal DLF, thus improving the interference suppression effect of the DL beamforming algorithm. Image features are easy to calculate, meaning that they have good ease of use in engineering applications. Because RDF-CB does not operate completely within the framework of traditional signal processing, it not only has a good interference suppression effect in nonideal situations, such as a small number of snapshots or DOA mismatch, but it also achieves improvement in interference suppression effect in special situations, such as a large number of sensor elements.

4. Discussion

4.1. The Advantages of RDF-CB

RDF-CB is capable of sensing the electromagnetic environment. The closed-loop structure from reception to perception to transmission is designed to emphasize the dynamic relationship between the external environment and the radar system. Unlike the existing beamforming methods based on variable DL, the RDF-CB method does not specify value rules for the DLF in the system beforehand. In fact, without prior knowledge of the RFI, it is difficult to determine a globally optimal DLF value rule. Taking the experimental results in Section 3.4 as an example, radical value rules will lead to the system falling into a local optimum. For example, the CS, GLC and LM methods underestimated the influence of the number of sensor elements, resulting in a generally small DLF. This made the covariance matrix load insufficient as the number of sensors increased and reduced the output SINR. Meanwhile, conservative value rules may limit the overall system performance. For example, the variation range of the DLF obtained via the CG method was relatively small. Although interference was suppressed under various conditions, the effect still had room for improvement. In contrast, RDF-CB used machine learning to pretrain the model and made better policy decisions with the help of a knowledge base.

RDF-CB can accurately describe the ionization environment from the perspective of image processing. By observing the RD maps, it can be found that the RFI had obvious image characteristics. The intensity of the interference and the effect of interference suppression could be intuitively perceived, which was the basis for our use of visual and image tools to process RD maps. However, the relationship between the image features and interference intensity was not simply linear. Reference [15] simplifies the corresponding relationship to monotonicity, thereby limiting the use of multidimensional image features and abandoning some valuable information. In general, inadequate image feature extraction will cause valuable information to be discarded. In RDF-CB, the mapping relationship between the

RD map and the DLF value is built by using an SVM and six-dimensional Tamura texture features. Rich RD map details can better distinguish the differences between different electromagnetic environments, including detailed features that are difficult to describe based on human experience.

An attention model is built into RDF-CB to screen for important information that is highly relevant to the DLF calculation. In the preliminary extraction of the Tamura texture features, each region of the RD map is treated as equally important, which is not fully consistent with the objective of the RFI suppression task. For OTHR application scenarios, RDF-CB weights the whole RD map with an attention model and gives more attention to the areas where RFI is prone to occur because these areas have the most influence on DLF selection.

4.2. Prospects and Limitations

The electromagnetic environment sensing system is one of the important components of a cognitive OTHR system [21]. Compared with traditional OTHR, the greatest difference in cognitive OTHR system architecture lies in the knowledge application function. In traditional OTHR, some key parameters of the transmitted signals are obtained through a series of external environmental sensing means, such as electromagnetic spectrum monitoring and ionospheric environment diagnosis. A very important gap between this and cognitive OTHR is the lack of feedback from receiver to transmitter. If environmental information can be extracted in the process of target detection, this can not only improve the efficiency of environmental perception but also allow environmental information to be introduced into the process of target detection, thus helping to improve the OTHR's target detection capability. Therefore, the above idea of designing transmitted signal parameters based on RD image feedback information has broad application prospects.

The RDF-CB method assumes that interference is suppressed in the ionospheric stationary state. The method focuses on the introduction of a cognitive interference suppression system, feature extraction methods, and machine learning prediction. However, the analysis and design of OTHR and the proposal of cognitive techniques depend on the monitoring and modeling of ionospheric conditions [20]. It is necessary to define the OTHR performance parameters in the actual ionospheric environment in order to control the feedback channel. Considering the influence of ionospheric phase contamination and multipath effects, the next step will be the fine modeling and actual testing of radar working scenarios. The influence of ionospheric conditions, the changes in the illuminated area and the clutter returns will be analyzed.

5. Conclusions

To address the problems that the traditional beamforming method is not capable of recognizing the electromagnetic environment and that its performance is greatly affected by the accuracy of signal feature estimation, RDF-CB for skywave radar was proposed. First, the RD map was weighted by local attention, and then, texture features were extracted for use as the input to an SVM. Finally, DLF prediction was performed using the SVM. Simulation results showed that this method had a good suppression effect for RFI and strong robustness, which is beneficial for engineering implementation. This combination of computer vision and machine learning also has the potential to be extended to other aspects of OTHR signal processing.

Author Contributions: Conceptualization, Z.L., Y.W. and H.C.; Data curation, Z.L. and Z.Z.; Validation, Z.L. and Z.Z.; Writing—original draft, Z.L.; Writing—review and editing, Y.W., H.C. and G.D. All authors have read and agreed to the published version of the manuscript.

Funding: This research was funded by the National Natural Science Foundation of China, grant number 62101593.

Data Availability Statement: Not applicable.

Conflicts of Interest: The authors declare no conflict of interest.

References

1. Jia, D.; Zhang, B.; Xie, J. Adaptive processing method for interference cancellation in skywave OTHR. *J. Eng.* **2019**, *2019*, 8103–8106. [CrossRef]
2. Li, Y.; Wu, L.; Zhang, N.; Wang, X. Constant false alarm rate detection based on estimating statistical distribution of non-homogeneous sea clutter in skywave over-the-horizon radar. *IET Radar Sonar Navig.* **2020**, *14*, 48–60. [CrossRef]
3. Luo, Z.; He, Z.; Chen, X.; Lu, K. Target location and height estimation via multipath signal and 2D array for skywave over-thehorizon radar. *IEEE Trans. Aerosp. Electron. Syst.* **2016**, *52*, 617–631. [CrossRef]
4. Zhang, Y.D.; Zhang, J.J.; Amin, M.G.; Himed, B. Instantaneous altitude estimation of maneuvering target in over-the-horizon radar exploiting multipath Doppler signatures. *EURASIP J. Adv. Signal Process.* **2013**, *2013*, 100. [CrossRef]
5. He, Q.; Li, X.; He, Z.; Blum, R.S. MIMO-OTH radar: Signal model for arbitrary placement and signals with non-point targets. *IEEE Trans. Signal Process.* **2015**, *63*, 1846–1857. [CrossRef]
6. Thayaparan, T.; Marchioni, J.; Kelsall, A.; Riddolls, R. Improved frequency monitoring system for skywave over-the-horizon radar in Canada. *IEEE Geosci. Remote Sens. Lett.* **2020**, *17*, 606–610. [CrossRef]
7. Fabrizio, G.; Colone, F.; Lombardo, P.; Farina, A. Adaptive beamforming for high-frequency over-the-horizon passive radar. *IET Radar Sonar Navig.* **2009**, *3*, 384–405. [CrossRef]
8. Carlson, B.D. Covariance matrix estimation errors and diagonal loading in adaptive arrays. *IEEE Trans. Aerosp. Electron. Syst.* **1988**, *24*, 397–401. [CrossRef]
9. Zhang, M.; Chen, X.; Zhang, A. A simple tridiagonal loading method for robust adaptive beamforming. *Signal Process.* **2019**, *157*, 103–107. [CrossRef]
10. Yu, L.; Fan, Y.; Wei, Y.; Xu, R. Robust adaptive beamforming method for large-scale array with automatic diagonal loading and steering vector estimation. *J. Eng.* **2019**, *2019*, 8047–8050. [CrossRef]
11. Li, W.; Zhao, Y.; Ye, Q.; Yang, B. Adaptive antenna null broadening beamforming against array calibration error based on adaptive variable diagonal loading. *Int. J. Antennas Propag.* **2017**, *2017*, 3265236. [CrossRef]
12. Gao, J.; Zhen, J.; Lv, Y.; Guo, B. Beamforming technique based on adaptive diagonal loading in wireless access networks. *Ad Hoc Netw.* **2020**, *107*, 102249. [CrossRef]
13. Song, A.; Wang, A.; Luan, S.; Qiu, T. Widely linear generalized sidelobe canceling beamforming with variable diagonal loading. *AEU Int. J. Electron. Commun.* **2017**, *76*, 77–85. [CrossRef]
14. Xiao, Y.; Yin, J.; Qi, H.; Yin, H.; Hua, G. MVDR algorithm based on estimated diagonal loading for beamforming. *Math. Probl. Eng.* **2017**, *2017*, 7904356. [CrossRef]
15. Wang, Z.; Luo, Z.; He, Z.; Shi, S. Coarseness in OTHR image and its application for diagonal loading factor determination. *IEEE Geosci. Remote Sens. Lett.* **2020**, *17*, 1523–1527. [CrossRef]
16. Osamy, W.; Salim, A.; Khedr, A.M. An information entropy based-clustering algorithm for heterogeneous wireless sensor networks. *Wirel. Netw.* **2018**, *26*, 1869–1886. [CrossRef]
17. Tamura, H.; Mori, S.; Yamawaki, T. Textural features corresponding to visual perception. *IEEE Trans. Syst. Man Cybern.* **1978**, *8*, 460–473. [CrossRef]
18. Wu, Q.; Zhao, Y.; Zhang, Q.; Jiang, B. Remote sensing image classification based on fusion of ATLTP and tamura texture features. *Int. J. Perform. Eng.* **2020**, *16*, 59. [CrossRef]
19. Imran, B. Content-based image retrieval based on texture and color combinations using Tamura texture features and Gabor texture methods. *Am. J. Neural Netw. Appl.* **2019**, *5*, 23–27. [CrossRef]
20. Fabrizio, G.A. High frequency over-the-horizon radar. In Proceedings of the IEEE Radar Conference, Boston, MA, USA, 22 April 2019.
21. Bao, Z.; Chen, J.; Qi, J. Study on ionosphere environment online sensing for cognitive over-the-horizon radar. In Proceedings of the CIE International Conference on Radar, Guangzhou, China, 13 October 2016.